THE UNIVERSITY OF
WARWICK

Original citation:
Barros, S. C. C., et al. ULTRACAM photometry of the ultracompact binaries V407 Vul and HM Cnc. Monthly Notices of the Royal Astronomical Society, 374(4), pp. 1334-1346.

Permanent WRAP url:
http://wrap.warwick.ac.uk/32495

Copyright and reuse:
The Warwick Research Archive Portal (WRAP) makes the work of researchers of the University of Warwick available open access under the following conditions. Copyright © and all moral rights to the version of the paper presented here belong to the individual author(s) and/or other copyright owners. To the extent reasonable and practicable the material made available in WRAP has been checked for eligibility before being made available.

Copies of full items can be used for personal research or study, educational, or not-for-profit purposes without prior permission or charge. Provided that the authors, title and full bibliographic details are credited, a hyperlink and/or URL is given for the original metadata page and the content is not changed in any way.

Publisher's statement:
'The definitive version is available at www.blackwell-synergy.com'.
DOI: 10.1111/j.1365-2966.2006.11244.x

A note on versions:
The version presented here may differ from the published version or, version of record, if you wish to cite this item you are advised to consult the publisher's version. Please see the 'permanent WRAP url' above for details on accessing the published version and note that access may require a subscription.

For more information, please contact the WRAP Team at: wrap@warwick.ac.uk

warwick**publications**wrap

highlight your research

http://go.warwick.ac.uk/lib-publications

ULTRACAM Photometry of the ultracompact binaries V407 Vul and HM Cnc

S.C.C. Barros[1]* T.R. Marsh[1], V. S. Dhillon[2] , P. J. Groot[3], S. Littlefair[2],
G. Nelemans[3], G. Roelofs[3], D. Steeghs[4] and P. J. Wheatley[1]

[1] *Department of Physics, University of Warwick, Coventry, CV4 7AL,UK*
[2] *Department of Physics and Astronomy, University of Sheffield,Sheffield , S3 7RH, UK*
[3] *Department of Astrophysics/IMAPP, Radboud University Nijmegen, P.O. Box 9010, NL - 6500 GL Nijmegen, The Netherlands*
[4] *Harvard-Smithsonian Center for Astrophysics, Cambridge, USA*

arXiv:astro-ph/0611117v1 3 Nov 2006

ABSTRACT
V407 Vul (RXJ1914.4+2456) and HM Cnc (RXJ0806.3+1527) are X-ray emitting stars with X-ray light curves that are 100% modulated on periods of 569 and 321 seconds respectively. These periods are thought possibly to represent the orbital periods of close pairs of white dwarfs. In this paper we present optical light curves taken with the high-speed CCD camera ULTRACAM on the 4.2m WHT in May 2003 and August 2005 and with the VLT in November 2005. The optical and X-ray light curves of HM Cnc have been reported as being in anti-phase, but we find that in fact the X-rays peak around 0.2 cycles after the maximum of the optical light, as seen also in V407 Vul. The X-ray/optical phase shifts are well explained under the accreting models of the systems if most of the optical modulation comes from the heated faces of the mass donors and if the X-ray emitting spots are positioned in advance of the mass donors, as is expected given the angular momentum of the accreting material. Some optical emission may also come from the vicinity of the X-ray spot, and we further show that this can explain the non-sinusoidal lightcurves of HM Cnc. On the basis of this model we constrain the temperature of the heated face of the companion star finding a bolometric luminosity $> 10^{33}$ ergs s^{-1} and a distance, $d > 1.1$ kpc. We can identify no explanation for the X-ray/optical phase-shifts under the intermediate polar and unipolar inductor models of the systems. The only significant difference between the two stars is that V407 Vul is observed to have the spectrum of a G star. The variation in position on the sky of a blend of a variable and a constant star can be used as a measure of their separation, and is sensitive to values well below the limit set by seeing. We apply this "pulsation astrometry" to deduce that the G star is separated from the variable by about 0.027″ and hence plays no role in the variability of V407 Vul. We show that light travel time variations could influence the period change in V407 Vul if it forms a triple system with the G star.

Key words: binaries: close– stars: individual: V407 Vul, HM Cnc – white dwarfs – stars: magnetic fields – X-rays: stars – astrometry

1 INTRODUCTION

V407 Vul (RXJ1914.4+2456 Motch et al. 1996) and HM Cnc (RXJ0806.3+1527, Israel et al. 1999; Burwitz & Reinsch 2001) were both discovered in the ROSAT all sky survey and have very similar X-ray properties. They have periods of $P = 569$ sec (Cropper et al. 1998; Motch et al. 1996) and $P = 321$ sec (Israel et al.

1999) respectively. In each star, only one period (and its harmonics) has been observed (Ramsay et al. 2000, 2002; Israel et al. 2002) at all wavelengths. Taken together, the observations have lead to a belief that the periods may be orbital, making these the shortest period binary stars known, and probably composed of pairs of white dwarfs. This would make these systems strong emitters of gravitational waves and possible progenitors or representatives of semi-detached AM CVn stars.

There are several rival models for these stars, all of them

based upon binary systems. The intermediate polar (IP) model (Motch et al. 1996; Israel et al. 1999; Norton et al. 2004) is the only one in which the pulsation periods are not assumed to be orbital. In this model, the pulsations are ascribed to the spin of white dwarfs accreting from non-degenerate secondary stars; the orbital periods are presumed undetectable. The other three models all invoke double white dwarf binaries in which the pulsation periods are the orbital periods. There is one detached model (i.e non-accreting), the unipolar inductor model (Wu et al. 2002), also called the electric star model because it is powered by the dissipation of electric currents induced by an asynchronism between the spin period of a magnetic white dwarf and the orbital period within a detached double white dwarf binary. The other two models each employ semi-detached, accreting double white dwarfs: one is magnetic, the double degenerate polar model (Cropper et al. 1998; Ramsay et al. 2002; Israel et al. 2002), while the other is non-magnetic, the direct impact model (Nelemans et al. 2001; Marsh & Steeghs 2002; Ramsay et al. 2002), in which, due to the compact dimensions of these systems, the mass transfer streams crash directly onto the accreting white dwarfs.

It has proved hard to decide which, if any, of the models is correct. Compared to typical accreting systems, HM Cnc has a weak optical line emission, while V407 Vul has none at all. This favours the unipolar inductor model which is the only one without accretion. The unipolar inductor model, along with the IP model, is also favoured by the observed decrease in pulsation periods (Strohmayer 2002, 2004; Hakala et al. 2003; Strohmayer 2003; Hakala et al. 2004) although recently accreting models with long-lasting spin-up phases have been developed (D'Antona et al. 2006; Deloye & Taam 2006). The shapes and phases of the X-ray light curves on the other hand count against the unipolar inductor model (Barros et al. 2005) which can only accommodate the high X-ray luminosity of V407 Vul with a white dwarf that spins faster than its orbit (Marsh & Nelemans 2005; Dall'Osso et al. 2006a,b). The accreting double-degenerate models on the other hand lead to high accretion rates and strong heating of the white dwarf, particularly in the case of HM Cnc, which is required to be at a distance of 4 to 20 kpc, and well out of the Galactic plane (Bildsten et al. 2006; D'Antona et al. 2006). At the moment therefore, there is no clear winner, or even leading contender amongst the models and better observational constraints are a priority.

Previous studies of the systems have focused mainly upon the properties of the X-ray light curves with optical data used mainly to track the decreasing periods with less attention being paid to the shapes of the light curves. With the work of D'Antona et al. (2006) and Deloye & Taam (2006) adding uncertainty to the interpretation of the period change measurements, the light curves themselves take on more significance. In this paper we present high-speed photometry of these systems in three simultaneous bands taken in the hope of using the optical characteristics to learn more about the systems. In section 2 we report our observations and data reduction. In section 3 we present our results. In section 4 we use our results to try to determine the origin of the optical pulses and explore the consequences for the accretion geometry in these systems.

Target	Date	UT	Seeing, clouds
V407 Vul	21 May 2003	05:33 - 06:25	1.0, clear
V407 Vul	22 May 2003	03:28 - 04:24	1.0, clear
V407 Vul	22 May 2003	04:54 - 06:25	1.0, clear
V407 Vul	23 May 2003	02:25 - 04:24	1.0, clear
V407 Vul	24 May 2003	02:48 - 03:41	1.0, some
V407 Vul	24 May 2003	04:50 - 06:18	1.0, clear
V407 Vul	25 May 2003	01:45 - 02:29	1.2, clear
V407 Vul	25 May 2003	03:19 - 04:41	1.2, clear
V407 Vul	27 Aug 2005	21:10 - 01:02	1.1, clear
V407 Vul	28 Aug 2005	21:05 - 22:38	0.9, clear
V407 Vul	30 Aug 2005	20:50 - 23:55	0.8, dusty
V407 Vul	31 Aug 2005	20:49 - 22:56	0.7, dusty
V407 Vul	01 Sep 2005	20:45 - 22:58	0.9, dusty
HM Cnc	21 May 2003	22:11 - 23:30	1.2, clear
HM Cnc	22 May 2003	21:54 - 22:57	1.0, clear
HM Cnc	23 May 2003	21:57 - 22:54	1.0, clear
HM Cnc	25 May 2003	21:55 - 22:39	1.3, clear
HM Cnc	27 Nov 2005	05:03 - 06:51	1.3, clear
HM Cnc	28 Nov 2005	05:10 - 08:47	1.0, clear
HM Cnc	29 Nov 2005	05:35 - 08:51	0.8, clear

Table 1. Observation log.

2   OBSERVATIONS AND REDUCTION

We observed with the high-speed CCD camera ULTRACAM (Dhillon & Marsh 2001) mounted on the 4.2m William Hershel telescope (WHT) in La Palma on May 2003 and August 2005, and mounted on the UT3 unit (Melipal) of the Very Large Telescope (VLT) in Chile in November 2005. For V407 Vul we have observations on five consecutive nights from the 21st to 25th of May, 2003 with a total of approximately 3600 frames of 9.7 sec exposure in the i', g' and u' filters and another 2000 frames of 15 sec exposure in five extra nights from the 27th of August to the 1st of September 2005 in r', g' and u'. For HM Cnc we have around 2000 frames taken in four nights from the 21st to 25th of May with 10.1 sec exposures in i', g' and u' and another 18,000 frames taken in November 2005 in r', g' and u' with exposures of 1 to 6 sec. The observing conditions are summarised in Table 1. All the times were transformed to TDB, and then shifted to time as observed at the solar system barycentre using the IDL routine *barycen* and recorded as a modified Julian day MJD(TDB).

The data were reduced using the ULTRACAM pipeline. We tried "optimal" photometry (Naylor 1998), variable aperture photometry and fixed aperture photometry to extract the light curves. Optimal photometry gave the higher signal-to-noise with the only exception the r' band in the August 2005 data, for which we used a fixed aperture radius. Optimal photometry requires the profiles to be identical in shape and can cause difficulties if this is not the case and we believe that in this one case this outweighed the improvement in stochastic noise. The subsequent data analysis was carried out with IDL. V407 Vul is in a crowded field so care was taken to prevent the sky annulus from being contaminated by other stars. It is trickier to allow for the faint stars that can contaminate the target aperture in poor seeing. These are a particular problem in the i' filter (May 2003 data) where we found the flux could increase by as much as 5% in the poorest seeing. Although relatively

few of the data were affected by this, we corrected for it by fitting and removing the trend of flux versus seeing from the i' data. Finally, the g' data from the second half of the second run of the 22nd of May 2003 and the second half of the second run of the 24th of May 2003 could not be used because V407 Vul was unfortunately positioned close to a column of poor charge transfer on the g' CCD.

In the May 2003 observations of V407 Vul we used two comparison stars, one (c1) for the i' and g' bands and the other (c2) for the u' images (because c1 was too faint in u'). The position relative to the target and the magnitudes of these comparison stars and the one used for HM Cnc are given in Table 3. In the August 2005 observations of V407 Vul we only used comparison star c2 because c1 was saturated in r' due to the longer exposure time. This run also suffered from Saharan dust that lead to an extra and variable extinction of ~ 0.5 magnitudes at the zenith making it impossible to derive an absolute calibration to better then 0.2 magnitudes. Therefore we used the g' and u' magnitudes of c2 calculated in May 2003 to calibrate the August 2005 data. To obtain the r' magnitude of c2 we applied the same correction as for g'.

The measured mean magnitudes of the systems are given in Table 2. As far as possible, the magnitude calibration was carried out by comparing the target and the comparison at the same airmass as we did not have sufficiently long runs to estimate accurate extinction coefficients. The uncertainties of the comparison star for HM Cnc are dominated by the uncertainties in the extinction coefficients for the night both in May 2003 (i) and in August 2005 (r, g and u) because in this case we did not observe the target and the comparison at exactly the same airmass and some correction was needed.

3 RESULTS

3.1 Ephemerides

To compare our optical data with the published X-ray data we had to fold our data, on the X-ray ephemeris. Unfortunately none of the ephemerides published so far (Strohmayer 2004, 2005; Israel et al. 2003, 2004; Ramsay et al. 2006) give the covariance terms of the fitted coefficients which are needed for a correct evaluation of the uncertainties. Therefore we had to digitise and fit the data of Strohmayer (2004, 2005) and Ramsay et al. (2006) so that we could obtain a timing solution whose uncertainties we could compare with our data. When we did this we realised that there was an inconsistency between the ephemerides of V407 Vul published by Strohmayer (2004) and Ramsay et al. (2006). After investigation we concluded that Strohmayer's (2004) ephemeris is probably in error because the ROSAT times were not corrected from UTC to TT. We therefore use our fitted Ramsay et al.'s (2006) ephemeris (Table A1) for V407 Vul which is similar to ephemeris given in Ramsay et al. (2006) but has a slightly different $\dot{\nu}$. For HM Cnc we used Strohmayer's (2005) ephemeris. Both ephemerides and respective covariance terms are given in Appendix A where we provide full details of our investigations.

Filter	Semi-amplitude (%)	$t - t_0$ (s)	ϕ (cycles)
i'	3.03±0.06	-4.9±1.8	0.9612±0.0032
g'	8.47±0.09	0.0±0.9	0.9698±0.0016
u'	20.50±0.61	3.9±2.7	0.9767±0.0047
r'	4.39±0.06	-0.7±1.2	0.9596±0.0021
g'	8.70±0.07	0.0±0.7	0.9607±0.0013
u'	21.64±0.44	0.0±1.8	0.9607±0.0033

Table 5. Results of single harmonic sinusoid fitting for V407 Vul. The first three lines show the results for the May 2003 data and the last three lines show the results obtained in August 2005. The times mark the position of the maximum phases and are $T_0 = 52782.191666$ for May 2003 $T_0 = 53612.9483393$ for November 2005. The phases are relative to the ephemeris of Table A1.

3.2 V407 Vul

We show our phase-folded light curves of V407 Vul folded on the ephemeris of Table A1 on the left of Fig. 1. The two datasets (May 2003 and August 2005) were rebinned to 100 phase bins using inverse-variance weighting to maximise the signal-to-noise ratio.

We computed the Lomb-Scargle periodogram (Lomb 1976; Scargle 1982) and confirmed the previously measured period of 569 sec. We then tested how close the signal is to a perfect sinusoid by fitting a sine wave at the fundamental frequency and at the second and third harmonics. The third harmonic is consistent with zero. The results for the relative amplitude and the phase at maximum of the fundamental (i.e. the "first harmonic") and the second harmonic are shown in Table 4 which also shows the corresponding results for HM Cnc. We also fitted a sinusoid with frequency fixed to the value derived from the ephemeris of Table A1 at our observing date to obtain a normalised amplitude of variation and the time (or equivalently the phase) of the maximum. The normalised amplitudes, the phase and the time-shifts relative to the g'-band are presented in Table 5. The amplitude increases strongly towards short wavelengths but there is no observable phase shift with wavelength. From Table 5 we calculate a difference of phase between our two runs of 0.0089 ± 0.002. This could be taken to be as a significant shift in phase, however the uncertainty only represents the measurement error. When we include the uncertainty of the ephemeris calculated with Equation A2 we obtain 0.0089 ± 0.019, and therefore we conclude that there is no significant variation of the phase shift between the optical and the X-rays between the two epochs of our observations and that the new ephemeris can be used to extrapolate to later times. To compare the optical phases with the X-ray light curves it is important to notice that the absolute error of the phase due to the ephemeris of Table A1 is 0.0090 for May 2003 and 0.019 for August 2005.

3.3 Pulsation astrometry of V407 Vul

A totally unexpected feature of V407 Vul is that its optical spectrum is dominated by that of a late G/early K star which cannot fit within a 10-minute period binary orbit (Steeghs et al. 2006). Although this immediately suggests the IP model in which one expects a main-sequence sec-

Target	i'	r'	g'	u'
V407 Vul May 2003	18.95±0.05	-	20.30±0.06	21.56±0.10
V407 Vul Aug 2005	-	19.3±0.1	20.29±0.06	21.53±0.08
HM Cnc May 2003	21.5±0.1	-	20.9±0.1	20.5±0.1
HM Cnc Nov 2005	-	21.21±0.10	20.77±0.11	20.51±0.12

Table 2. Magnitudes measured for the two targets.

Comparison	$\Delta\alpha$ arcsec	$\Delta\delta$ arcsec	i'	r'	g'	u'
V407 Vul c1	+3.1	-8.4	14.21±0.01	saturated	16.26±0.01	19.78±0.03
V407 Vul c2	+39.5	-37.0	15.73±0.01	16.08±0.1	16.96±0.01	18.84±0.03
HM Cnc	-16.9	-16.4	15.25±0.11	15.31±0.10	16.00±0.11	17.73±0.12

Table 3. Positions relative to the target and magnitude of the comparison stars used to flux calibrate the data.

ondary star (Norton et al. 2004), the star shows no radial velocity variations at a level that rules out orbital periods typical of cataclysmic variable stars ($\leq$ 1day, Steeghs et al. 2006). Alternatives are that this star is a line-of-sight coincidence (the field is a crowded one), or it could be part of a triple system with the variable. To discriminate between the latter possibilities we searched for variations in the position of V407 Vul on its 569 period. The idea behind this "pulsation astrometry" is that although we cannot spatially resolve the variable and G star components of V407 Vul directly, we can use the pulsations of the variable to try to detect their separation because their mean position will move back and forth between the variable and the G star as the variable brightens and fades. This method is sensitive to separations well below the seeing.

We measured the position of V407 Vul relative to nearby stars in the field. We then computed the amplitude of the best-fitting sinusoid over a range of frequencies for both the x- and y-positions in each of the three filters as shown in Fig. 2. We computed false alarm probabilities using Monte Carlo simulations (finding values that agree with the theoretical values of Schwarzenberg-Czerny 1998). In Fig. 2 we show the 99.9% detection threshold for a known period (horizontal solid lines) and also the 99.9% detection threshold for an arbitrary unknown period (dashed lines). We choose the 99.9% level because it corresponds to a detection limit of about "3σ". Note that the detection criterion is more stringent when we don't know the period because a penalty must be paid for searching multiple independent periods (Horne & Baliunas 1986). We include this level to show that there are no such detections of any other periodicities. In the case of V407 Vul we know the period that we are looking for so it is the lower threshold represented by the solid lines that applies. As mentioned above, the g' data of the May 2003 run were partially affected by poor charge transfer in a column close to V407 Vul. This has more of an effect upon position (especially at the levels we measure here) than on flux, so for the position measurements we discarded the 50% of the g' data where V407 Vul was closest to the column, but as a result reduced the sensitivity of the g'-band data in the left-hand side of the figure.

There are detections of a signal at the 99.9% level in the y-position data in both r' and g' of the August 2005 run.
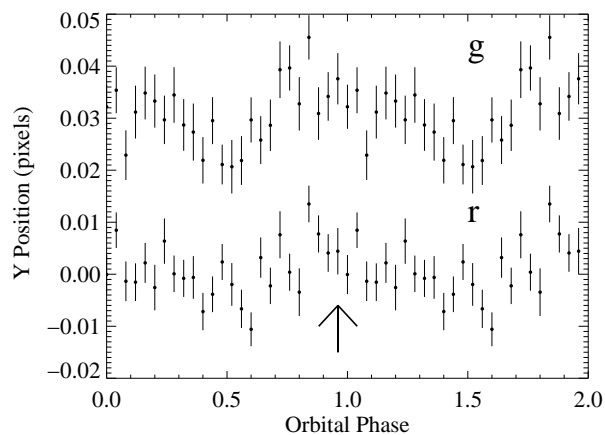

Figure 3. Phase folded position variation for g' and r' the datasets that show a significant signal. The arrow shows the position of the maximum of the flux.

Fig. 3 shows a phase-folded, binned plot of the y-position for these two cases. The time of maximum excursion roughly corresponds with the time of maximum light as expected, and both datasets are consistent with each other in this respect. However, the signal is tiny, with an amplitude of just 0.005 pixels or 0.0015 arcsec, and so we endevoured to test the reliability of this detection as far as we were able. The most obvious problem is that V407 Vul is in a crowded field and so the position measurements could be affected by other stars. There are two stars within 1.5 arcsec of V407 Vul that can be seen in Figure 2 of Ramsay et al. (2002). To check how these stars affected our measurements we first tested whether the detection depended upon the FWHM of the seeing. We divided the data in two parts, higher and lower FWHM. The reduction of data size lead to no detection in either case but the significance of the peaks was higher in the small FWHM dataset. The reverse would have been expected had blending with the two nearby stars been the cause.

We measured the centroids by cross-correlation with 2D Gaussians of fixed width. This allows us to assess the effect of the Gaussian width upon the measured amplitude. As the
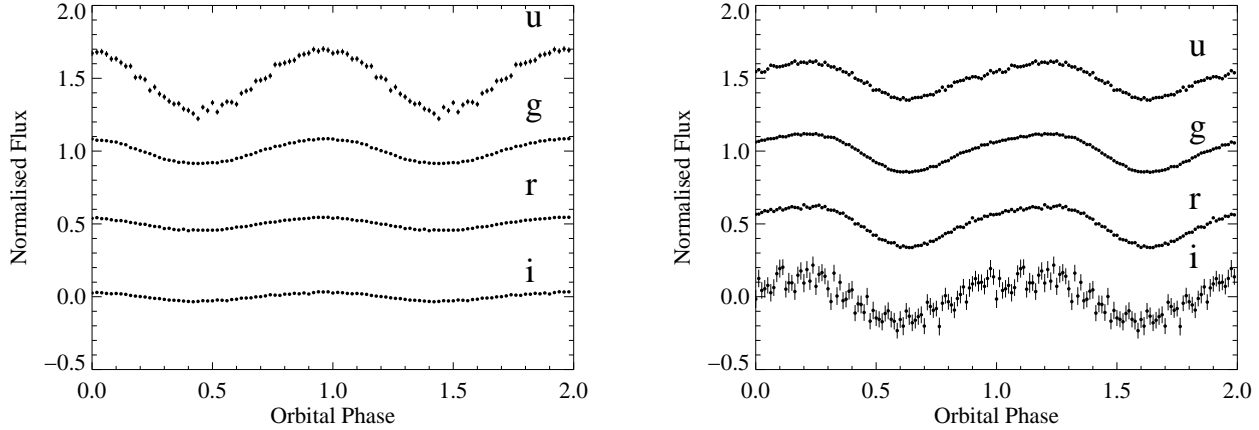
Figure 1. Phase-folded light curves of V407 Vul (left) and HM Cnc (right) using Table A1 and Strohmayer's (2005). The flux is normalised to unity in each case. The different filters are displaced vertically for clarity.

Filter	V407 Vul			HM Cnc		
	a_2/a_1	ϕ_1	ϕ_2	a_2/a_1	ϕ_1	ϕ_2
i'	0.079±0.030	0.961±0.012	0.458±0.16	0.207±0.064	0.122±0.010	0.335±0.025
g'	0.053±0.014	0.970±0.005	0.388±0.08	0.157±0.025	0.117±0.004	0.338±0.012
u'	0.095±0.036	0.977±0.012	0.544±0.05	0.131±0.050	0.118±0.008	0.285±0.031
r'	0.024±0.015	0.960±0.020	0.361±0.099	0.202±0.009	0.1616±0.0014	0.362±0.0034
g'	0.039±0.012	0.961±0.013	0.444±0.14	0.188±0.005	0.1659±0.0008	0.356±0.0022
u'	0.012±0.022	0.961±0.033	0.340±0.27	0.205±0.014	0.1700±0.0022	0.342±0.0055

Table 4. First and second harmonic decomposition of the optical light curves for V407 Vul and HM Cnc. a_1 and a_2 are the semi-amplitudes of the first and second harmonics respectively and ϕ_1 and ϕ_2 their phases of maximum light on Table A1's and Strohmayer's (2005) ephemeris. In the case of HM Cnc, the measurements at the top and bottom come from the WHT and VLT respectively, hence the marked difference in the uncertainties.

FWHM of the Gaussian increases, we expect to see a more pronounced impact of the nearby stars. Therefore if it is the nearby stars rather than the G star that are responsible for the variation, we expect an increase of measured amplitude with Gaussian width. In fact we see the reverse as Fig. 4 shows, at least in the y-positions for which we have detections. The x positions do show a distinct upturn at large FWHM owing to the much brighter star 5″ East of V407 Vul (star B of Ramsay et al. 2002) which was positioned to the left of V407 Vul in our data.

As a final check we carried out simulations of our position measurements using parameters matching the stars that we could see nearby V407 Vul, including the two very close ones mentioned above. This leads to the dotted line in Fig. 4. In viewing this figure it must be recognised that the data are not independent and so to some extent the trends with FWHM can just reflect noise; the dashed lines in the figure show two simulations of the effect that noise can have upon the simulated amplitudes. These show that for the y-positions the measured amplitudes are indeed significantly larger than the simulated values, and provide further confidence in the reality of the detection.

We conclude, albeit tentatively, that we have detected a change in the spatial position of V407 Vul that is correlated with its pulsations and that the change in position is
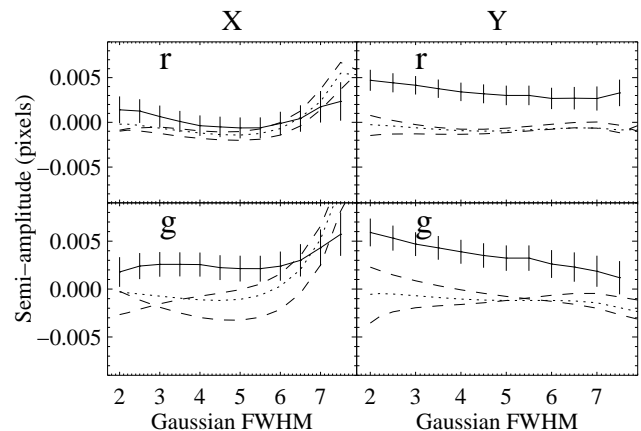

Figure 4. The dependence of the amplitude of the variation of the position upon the width of the Gaussian used to calculate the position. The data are plotted as a solid line, the simulations accounting for the known stars are plotted as dotted lines (no noise) and dashed lines (with noise). The simulations with noise have similar errors to the data but these errors were not plotted for clarity. The plate scale is 0.3" per pixel.

because the G star we see in its spectrum is not exactly coincident with the variable. We predict that the G star should be below V407 Vul in our field which roughly corresponds to south of V407 Vul. We obtain amplitudes of the posi-
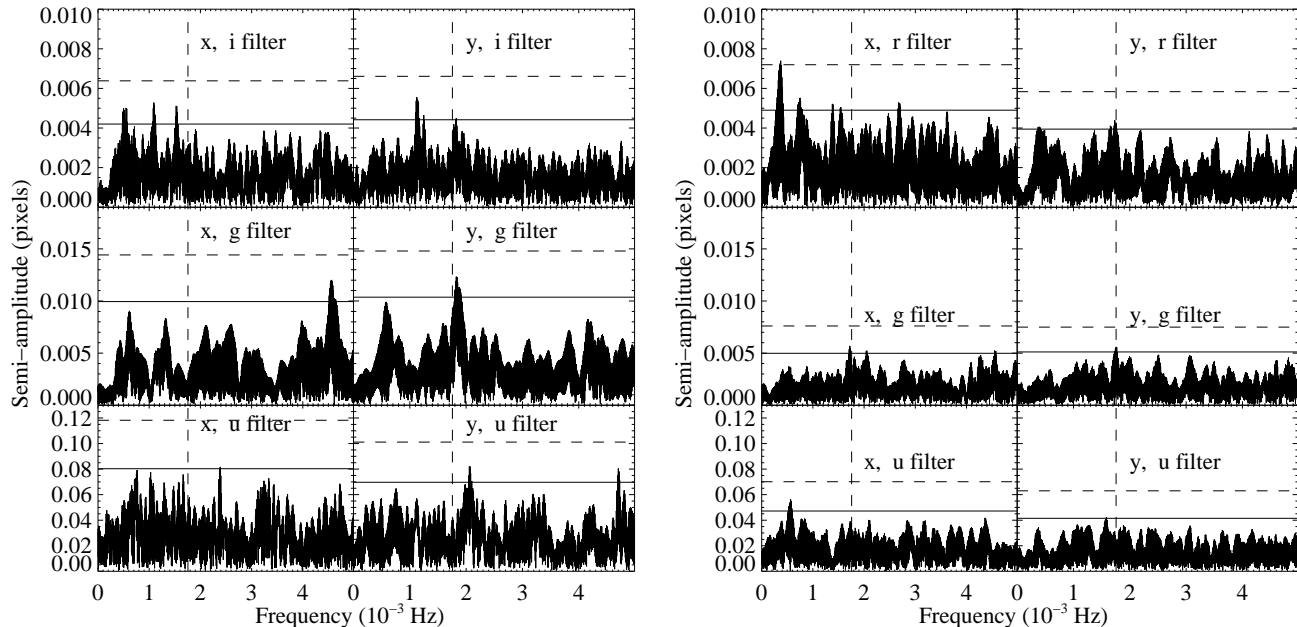
Figure 2. Each panel shows the amplitude spectra of the x (left) and y (right) variation of the position of V407 Vul for the three filters i' or r', g', and u' from top to bottom. The left panel shows the May 2003 data while the right shows the August 2005 data. The vertical dashed lines show the position of the 569 sec period. The solid horizontal lines show the 99.9 percent significance level for a known period and the dashed horizontal lines show the same level for an arbitrary period.

tion variation which we denote by p of 0.00512 ± 0.0012 and 0.00514 ± 0.0010 pixels for g' and r' respectively.

The value of p is related to the separation on the sky d, the fractional amplitude of the flux variation a as listed in Table 5 and the fractional contribution of the G star to the flux at minimum light f, through the following relation:

$$p = \left(\frac{a}{a+1}\right) fd. \qquad (1)$$

Using the measured values for a and p we calculate $f_{r'}d = 0.0366'' \pm 0.0073$ and $f_{g'}d = 0.0192'' \pm 0.0046$. This gives a value of $f_{g'}/f_{r'} = 0.52 \pm 0.16$. This is consistent with the spectra of the G star from which Steeghs et al. (2006) estimate that $f_{r'} > 0.85$ and $f_{g'} > 0.6$. These numbers also match the amplitude of the flux variation whose significant drop from u' to g' to r' (Table 5) can be explained by dilution of an underlying variable with a constant amplitude with wavelength, as for HM Cnc. If we assume $f_{g'} = 0.7$ we obtain $d \sim 0.027''$; this compares with the upper limit of 0.1" set by Steeghs et al. (2006). The distance to the G star of 1 kpc estimated by Steeghs et al. (2006), leads to a minimum separation of ~ 30 AU, equivalent to a period of 120 yr, and means that the G star cannot be the direct cause of the optical and X-ray pulsations. Nevertheless it may well be associated with the system in the form of a hierarchical triple, a point we return to after we have presented the lightcurves of HM Cnc. We finish by noting that our failure to detect anything in the u' band is to be expected. Assuming typical colours for the G star and a hot spectrum for the variable, we expect that if $f_{g'} = 0.7$, then $f_u' = 0.3$. The effect of this reduction in f, which is to make any movement more difficult to detect is in large part offset by a factor 2.1 increase in $a/(1+a)$, but then we are faced with a factor 8 worse

sensitivity in the u' band, and the result is that there is no detection in the u' band data.

3.4   HM Cnc

We present the phase-folded light curves of HM Cnc using Strohmayer's 2005 ephemeris in the right-hand panel of Fig. 1.

We computed the Lomb-Scargle periodogram to confirm its 321 sec period and we noticed that the relative strength of the second harmonic is higher than V407 Vul's, as has already been pointed out by Israel et al. (2002). This is indeed clear from the non-sinusoidal shape of the light curves in Fig. 1. The results of the relative strength of the first and second harmonic and their phases are shown in Table 4. The second harmonic is approximately 15% of the fundamental and its maximum occurs 0.2 of a cycle after the maximum of the fundamental. This results in an asymmetry in the light curve whose rise time is longer than its decline; we discuss its origin in section 4.

We applied the same method as for V407 Vul to obtain the normalised amplitude of variation and the time and phase of the maximum. These results are presented in Table 6. In this case the amplitude of the variation decreases slightly for shorter wavelengths which reinforces the picture that in V407 Vul the change with wavelength is due to dilution at long wavelengths by light from the G star. For HM Cnc the normalised amplitudes of variation are smaller than the u' band for V407 Vul (which is the least contaminated by the constant star). This could be easily explained by the inclination of the plane of the orbit and/or differences in temperatures of the stars.

The higher signal-to-noise ratio of the VLT data from November 2005 reveals a trend with waveband in the phase

Filter	amplitude (%)	$t - t_0$ (s)	ϕ (cycles)
i'	14.77±0.95	1.7±3.2	0.121±0.010
g'	13.48±0.34	0.0±1.3	0.116±0.004
u'	13.08±0.66	0.5±2.6	0.118±0.008
r'	13.54±0.12	-1.30±0.45	0.1615±0.0014
g'	12.74±0.07	0.00±0.27	0.1656±0.0009
u'	11.90±0.17	1.32±0.72	0.1697±0.0023

Table 6. Results of single harmonic sinusoid fits to the HM Cnc data. The times mark the phases of maximum light and are referenced to two times: $T_0 = 52782.895768$ for the May 2003 data and $T_0 = 53702.3368167$ for the November 2005 data.
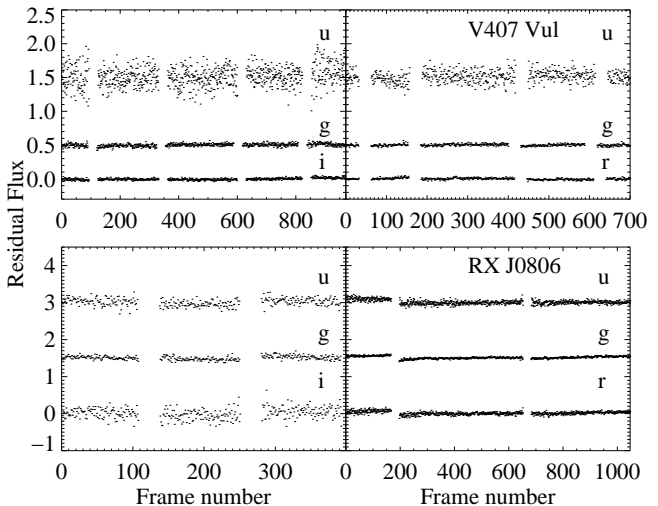

Figure 6. V407 Vul (top panel) and HM Cnc (bottom panel) light curves after removal of the sinusoidal pulsations. For each object the data from the first observing period is in the left and the second in the right. There are no significant variations of either source. We inserted gaps between different nights.

of the fundamental which is progressively delayed towards short wavelengths. To test whether the trend is significant, we carried out an F-ratio test comparing two models, one of a constant phase in the three bands versus one of a linear trend of phase with wavelength, using the central wavelengths of each band: 3543, 4770 and 6222 Å. The F-ratio is the ratio between the χ^2/(number of degrees of freedom) of one fit divided by the same quantity for the other fit. We only had three points so the constant model has two degrees of freedom while the straight-line fit has just one. The values of the χ^2 are 10.82 and 0.068 for the constant and straight-line respectively, giving an F-ratio of 79.5. This is significant at the 90% level but not at 95%, so, although suggestive, there is no significant shift.

Table 6 shows that there is a phase difference of 0.050 ± 0.004 between our two runs (May 2003 to November 2005) where this is the measurement error only. As with V407 Vul, we also have to add the uncertainty of the ephemeris (see the appendix). The error of the difference of phases due to the uncertainty of the ephemeris calculated using Equation A2 and the correlation coefficients given in Table A2 is 0.013. So there is a phase difference between the two runs of 0.050 ± 0.014. Therefore there is marginally significant variation in phase which might mean that there is a variation of the phase shift between the optical and the X-rays or, more likely, that the spin up rate is varying. The uncertainty in the absolute phase calculated using Equation A1 is 0.005 for the May 2003 data and 0.01 for the November 2005 data. These are useful to compare the optical phases with the X-ray phases, and as we shall see next there is a significant phase shift between the two.

3.5 The Optical/X-Ray phase shift of HM Cnc

The relative phases of the optical and X-ray light curves are an important constraint upon models. Israel et al. (2003, 2004) found that optical and X-ray light curves of HM Cnc were in anti-phase as might be expected for an X-ray emission region facing the secondary star, contrary, for example, to expectations based upon the direct impact model.

In the right-hand panel of Fig. 5 we present the X-ray and optical light curves folded on Strohmayer's (2005) ephemeris. Our phase shift differs from Israel et al.'s (2003; 2004) studies by around 0.2 cycles. To test if this was a genuine change in the system, we reduced some of the archival R-band VLT data from the 12th of December 2002 used

by Israel et al. (2004). We reduced these data with the UL-TRACAM pipeline and applied the same methods and time conversions as for the WHT/ULTRACAM data. The results are also shown in the right-hand panel of Fig. 5 and agree nicely with our ULTRACAM data. Clearly the system phase is stable and there are no problems with the times of either data set. The difference must be due to the data reduction. We confirmed our timing results with three different data reduction packages so we believe that our relative phase is correct and suspect that there is a problem with Israel et al.'s (2003; 2004) values. We were able to confirm Israel et al.'s (2003; 2004) X-ray phase so assume that there is a problem only with the optical timings. The shift of 0.2 cycles is about 1 minute, which is suggestively close to the ~ 64 seconds offset between UTC and TDB. Dr Israel was kind enough to confirm that such an error was possible.

3.6 Flickering

The random stochastic variations known as "flickering" are one of the hallmarks of accreting systems. We therefore looked for any signs of flickering in our data. A plot of the light curves after removing the sinusoidal variation is shown in Fig. 6.

The light curves are very constant except for long timescale variability of HM Cnc during the November VLT run. The observations of HM Cnc started at high airmass, so some of variations seen could be a consequence of extinction, except that u' does not look much more variable than g' or r'. Therefore we believe that this may be true variability of the source and not an artefact.

In both systems the magnitudes measured in the two observing runs agree well within the errors. In the case of V407 Vul we also searched for any flux variation on longer time scales. We had data from the "auxiliary port" of the WHT taken on the 10th of April 2003 and also Liverpool Telescope data taken on the 5th of September 2004. The different data sets were all within 10% of each other.
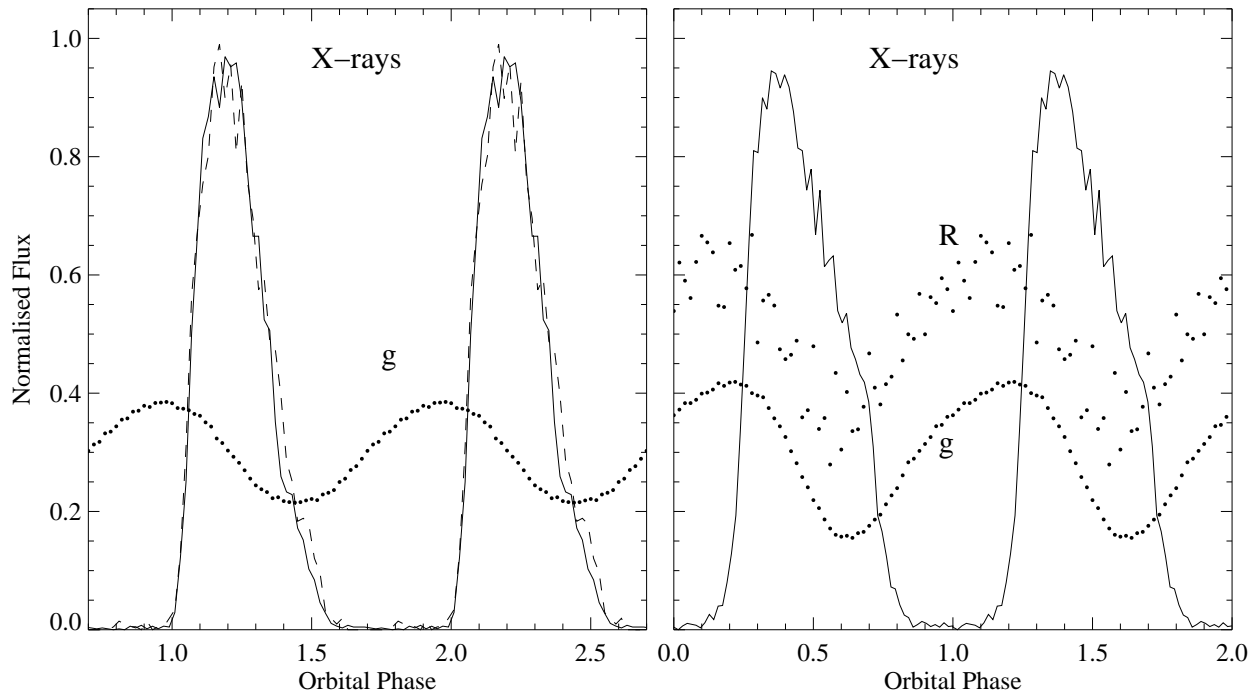
Figure 5. X-Ray/optical phase folded light curve of V407 Vul (left) and HM Cnc (right) using the ephemeris of Table A1 and (Strohmayer 2005) respectively. For the X-ray light curves of V407 Vul we re-analysed Chandra observations, with the solid line showing data from 19th February 2003 and the dashed line from 24th November 2003. For HM Cnc, the X-rays were adapted from Strohmayer (2005). We overplot the optical g' band showing our results. For HM Cnc we also show the VLT/FORS data (Israel et al. 2002) taken in the R filter (top).

We estimated the variability of these systems by calculating the RMS of the lightcurves after removing the sinusoidal variations. We filtered the short-term variations to minimise the photon noise. We also filtered longer term variations so we could compare our short runs with a longer run on the cataclysmic variable SS Cyg. For the August 2005 V407 Vul run we obtain an RMS variability of 0.7% in r' and 0.8% in g'. For the November run on HM Cnc we obtain an RMS variability of 1.6% in r' and 1.0% in g'. We use these runs as they have the highest signal-to-noise, nevertheless the variability still contains a significant component of photon noise. We do not quote the variability in u' because it is completely dominated by photon noise. For comparison, applying the same filtering of the data to data on the well-known CV SS Cyg, we obtain an RMS variability of 3.0% in r' and 5.0% in g'. As mentioned above, the fraction of the G star in the g' band of V407 Vul is of order 70%. Therefore its intrinsic variability is of order 2.5%, assuming the variations are not dominated by photon noise. This is a factor of two less than SS Cyg and a factor of four if one accounts for SS Cyg's dilution by its secondary star (North et al. 2002). Other cataclysmic variable stars we looked at are similar to SS Cyg, so we conclude that the measured variability in V407 Vul and HM Cnc is much less than in normal cataclysmic variable stars.

The lack of obvious flickering is a point against accreting models, although not a conclusive one as there are wide variations in the amount of flickering shown by definitively accreting binaries, and one cannot be certain that it should have been detected. It does however suggest that most of the optical light does not come directly from the accreting region.

4   DISCUSSION

4.1   The X-ray versus optical phases

The correction to the relative X-ray versus optical phase of HM Cnc that we have identified makes it very similar in this respect to V407 Vul: in each system the X-ray flux peaks ~ 0.2 cycles after the optical flux. This can be added to the shapes of the light curves as evidence that these two stars are indeed related systems, as is evident from Fig. 5. We will now investigate what this result implies for the different models.

In the majority of models, the X-rays come from a spot on the primary star which moves in and out of view as it rotates. The exception is the IP model where the modulation is the result of the accretion stream flipping from one pole to the other although it seems unlikely that such a process can really switch off the X-rays as completely as observed. Less attention has been paid to the optical pulsations. Within double degenerate models, these seem likely to

originate from the heated face of the secondary star which would naturally explain their near-sinusoidal shape and, perhaps, the absence of flickering. Such heating may be a result of the X-ray emission from the primary star, or the primary star could simply be hot as a result of compressional heating (Bildsten et al. 2006).

Assuming that we are correct about the main site of optical emission, Fig. 7 shows the geometrical arrangement that explains the relative phases of the optical and the X-ray light curves. In this model the 0.2 cycles delay of the X-ray peak relative to the optical peak implies that the X-ray emission spot is rotated ~ 0.3 cycles from directly facing the secondary star, in the direction of the orbit.

This is not the whole story however, because in HM Cnc at least the optical light-curve is somewhat saw-toothed in shape. As our Fourier decomposition shows, this is caused by a significant second harmonic that happens to peak at the same phase as the X-rays, as seen in the difference $\phi_2 - \phi_1 \approx 0.2$ in Table 4. The natural explanation for this is that the X-ray emission spot is also the site of some optical light. If this is a localised region so that the shape of its light curve can be approximated by a truncated sinusoid ($f(\theta) = \cos\theta$ for $-\pi/2 < \theta < \pi/2$, $f(\theta) = 0$ otherwise), then it can produce a second harmonic. It will also contribute some first harmonic as well, which means that the first harmonic emission that we see is the combination of contributions from the heated face of the secondary star and the spot on the primary star. This retards the optical phase so that the observed 0.2 cycle shift is an under-estimate of the true shift between the emission from the heated face and the X-ray emission.

If the optical emission truly can be approximated by the truncated sinusoid, then for HM Cnc we find that we can fit the phases and harmonic amplitudes if the X-ray spot leads the heated face of the secondary star by ~ 0.26 cycles (i.e. a little more than $90°$) and the optical emission from the spot on the primary star peaks at $\sim 75\%$ of the amplitude of the emission from the heated face. While this is probably rather simplistic, it demonstrates that the simple model illustrated in Fig. 7 is capable of explaining some secondary details of the data. With this decomposition of the optical light, the X-ray emission site is $\sim 90°$ ahead of the secondary star and it is then not clear if the X-rays can directly heat the secondary star or not. V407 Vul has a much weaker second harmonic, and so in this case the spot is presumably the full 0.3 cycles or $\sim 110°$ ahead of the secondary star and cannot see it directly.

The X-ray/optical phase-shifts in V407 Vul and HM Cnc are very naturally explained by both the direct impact and double-degenerate polar models. The accretion spot in normal polars is observed to lead the secondary star by of order 0.1 to 0.3 cycles (Cropper 1988) and a similar shift is expected in the direct impact model, depending upon the system parameters (Marsh et al. 2004). As Fig 7 shows, this is exactly what is required to match the observations. On the other hand, as far as we can see, there is no natural explanation for the phase-shift in the unipolar inductor model for which one would expect anti-phasing, unless there is some as yet undiscovered mechanism for displacing the magnetic footprint of the secondary star in advance of its orbit. This is difficult given that the orientation of the primary star relative to the secondary star changes relatively

rapidly in the unipolar inductor model and so a fixed orientation is hard to contrive. The X-ray/optical phase-shift is also a difficulty for Norton et al.'s (2004) IP model for which they also predict anti-phasing with the optical pulses appearing as the accretion stream switches to the hidden pole, the X-rays going to zero at this point. IPs are sufficiently complex that an offset as observed would not perhaps be that surprising, but in any case there are other more serious difficulties with the IP model (Cropper et al. 2004).

The direct impact model can be used to predict the phase shape and thus, if it is true, constrain the masses of the binary components. We define the impact angle as the angle between the X-ray emission site and the secondary star. We calculate the impact angle for over a grid of M_1 and M_2. In Figure 8 we show contours of same impact angle where the shaded areas represent the probable regions where the systems lie. The uncertainties in the angle are higher for HM Cnc than for V407 Vul because of the existence of the second harmonic component. In the same figure we also plotted the dynamic stability limit (dashed line). We conclude that for V407 Vul $0.4 < M_1 < 0.55\,\mathrm{M_\odot}$ and $0.08 < M_2 < 0.4\,\mathrm{M_\odot}$ and for HM Cnc $0.6 < M_1 < 0.9\,\mathrm{M_\odot}$ and $0.12 < M_2 < 0.45\,\mathrm{M_\odot}$.

4.2 A limit on the bolometric luminosity of HM Cnc

Pursuing the idea of the heated face further leads to a lower limit upon the bolometric luminosity of HM Cnc, assuming that the double degenerate models are correct (unfortunately the G star in V407 Vul's spectrum precludes the same calculation). The idea is to derive a lower limit on the temperature of the heated face from the spectrum of the pulsations, which since it is a measure of the flux from the primary star at a distance equal to the orbital separation, which is approximately known, gives us a luminosity. A slight complication is that we do not know for sure whether the X-rays or the primary star's photosphere is responsible for the irradiation. This ultimately leads us to two different possible limits. We begin by obtaining the weaker of the two which applies in the case of X-ray heating, and then consider the revised limit necessary if the photosphere is responsible for the heating.

4.2.1 Temperature of the heated face

We first derive a lower limit on the temperature of the spectrum using our magnitudes and those reported by Ramsay et al. (2002), Israel et al. (2002) and Reinsch et al. (2004), as shown in the left-hand panel of Fig. 9. Two blackbody spectra are shown, each scaled to give the minimum χ^2. One, with temperature 32,400 K (solid line) is the global best fit, while the other (dotted), with temperature 18,500 K, has the minimum temperature that gives a χ^2 within the 99% confidence threshold. We take this to be the minimum possible temperature of HM Cnc given its optical and infra-red fluxes. We assume further that this reflects the temperature of the primary star, T_1, since if it is the secondary star, the primary star would have to be extremely hot to produce a significant reflection effect; there is no equivalent upper limit as the optical and IR fluxes do not constrain the maximum temperature at all. Armed with the lower limit of
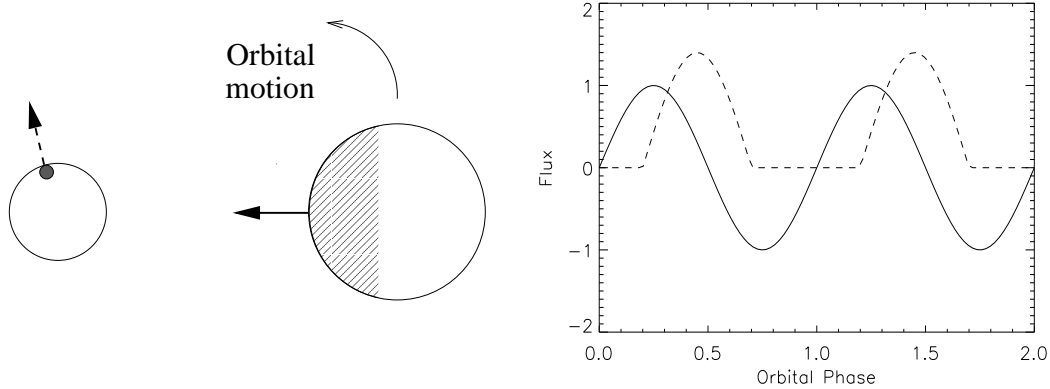
Figure 7. In the left-hand panel we show a schematic picture of the primary star (left) with an X-ray emitting spot which has a peak of X-ray emission in the direction indicated by the dashed arrow. The relative sizes of the two stars are drawn to match masses of $M_1 = 0.53\,\mathrm{M}_\odot$ and $M_2 = 0.12\,\mathrm{M}_\odot$ (see text). The secondary star, which orbits counter-clockwise, has a heated face (shaded) whose peak emission is in the direction of the solid arrow. The figure is arranged to give the optical (solid) and X-ray (dashed) light curves shown on the right, which have the same relative phasing as both V407 Vul and HM Cnc.
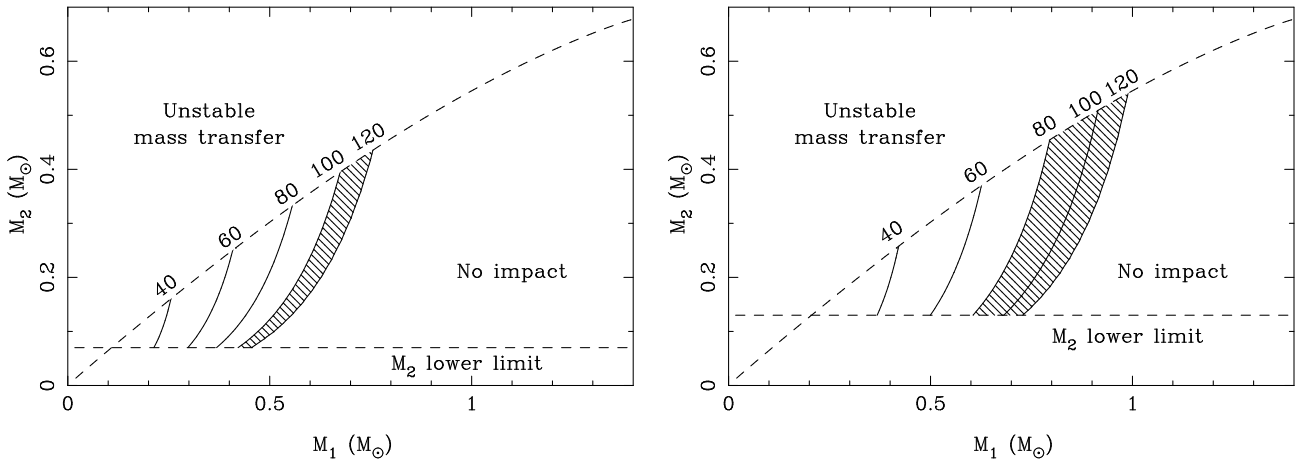
Figure 8. We show the system mass constraints for V407 Vul (left-hand panel) and HM Cnc (right-hand panel) if we assume the direct impact model. The upper dashed line shows the dynamic stability limit. We show contours of equal impact angle. Note that the maximum impact angle is approximately 130° which corresponds to the transition between the disc and direct-impact accretion.

$T_1 > 18,500\,\mathrm{K}$, we can then use the pulsation amplitudes to place a similar lower limit upon the temperature of the irradiated face of the secondary star T_{irr} using the ratio of black-body spectra, as shown on the right of Fig. 9. Again taking the 99% confidence limit, we find that the temperature of the irradiated face must be at least $T_{\mathrm{irr}} > 14,800\,\mathrm{K}$; this limit rises to 21,700 K if we use the best-fit value for T_1 of 32,400 K. The lower limit on the temperature of the irradiated face leads directly to a lower limit on the bolometric luminosity of the primary star since assuming that the irradiation dominates the intrinsic luminosity of the secondary star we have

$$L_{\mathrm{bol}} = 4\pi a^2 \sigma T_{\mathrm{irr}}^4, \tag{2}$$

where a is the separation and σ is the Stefan-Boltzmann constant. The strictest lower limit comes from taking the smallest separation, which corresponds to the smallest masses for the two component stars. We used $M_1 = 0.53\,\mathrm{M}_\odot$ and $M_2 = 0.12\,\mathrm{M}_\odot$ which ensure that the secondary star can

fit within its Roche lobe and that mass transfer is stable (Marsh et al. 2004); a smaller value for M_1 could be used if the system is detached, but would be largely compensated for by the need for a higher value of M_2 to avoid mass transfer. Our masses and the period of 321 seconds imply a separation of $a = 0.089\,\mathrm{R}_\odot$ (these values were used to scale Fig. 7). Scaling from the Sun we therefore find that $L_{\mathrm{bol}} > 0.34\,\mathrm{L}_\odot = 1.3 \times 10^{33}\,\mathrm{ergs\,s^{-1}}$.

This is already a significant lower limit as it is somewhat higher than, but consistent with, the X-ray luminosity of $L_X \sim 5 \times 10^{32}\,\mathrm{ergs\,s^{-1}}$ at 500 pc distance estimated by Israel et al. (2003). However, we have pushed the temperature to marginally acceptable values. For instance, the best-fit temperature $T_1 = 32,400\,\mathrm{K}$ which leads to $T_{\mathrm{irr}} > 21,700\,\mathrm{K}$ raises the luminosity limit by a factor of 4.4, which hints at a larger distance than Israel et al. (2003) assumed.

Comparing with white dwarfs of similar temperature and mass (Bragaglia et al. 1995), the absolute magnitude of the primary star is bounded by $M_V < 10.7$. Given $V = 21.1$
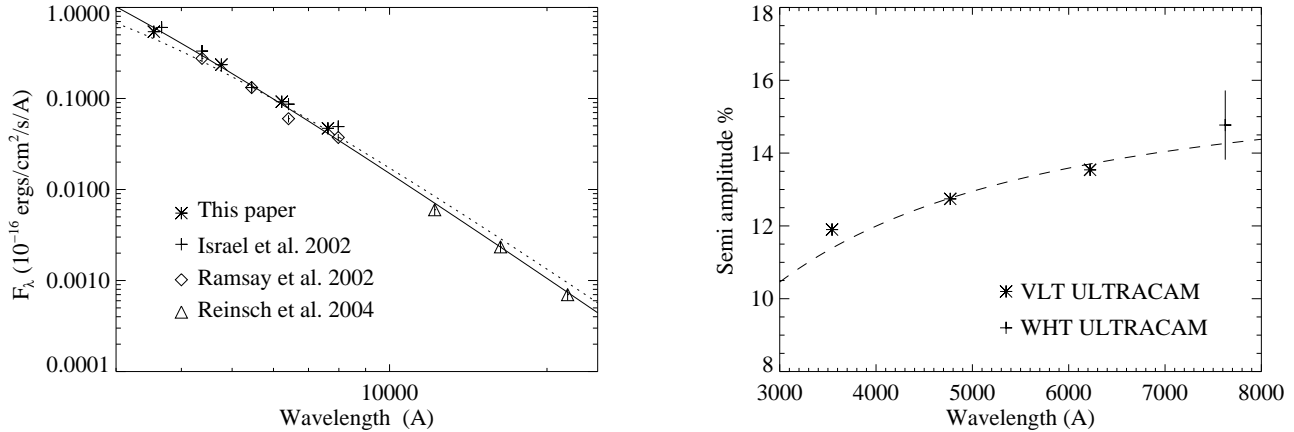
Figure 9. In the left-hand panel we show the mean fluxes of HM Cnc compared to two black-body spectra. One is the best fit (32,400 K, solid), the other has the lowest temperature consistent with the data ($T_1 = 18,500$ K, dotted). The right-hand panel shows the pulsation amplitudes that we measure compared to the ratio of two black-bodies ($B_\lambda(T_{irr})/B_\lambda(T_1)$) to place a lower limit upon the temperature of the pulsed light $T_{irr} > 14,800$ K; the dashed line shows the limiting case.

(Israel et al. 2002), and assuming that reddening is negligible, this suggests that $d > 1.1$ kpc, although this limit can be lowered if we adopt a higher mass for the primary star.

These limits apply if it is the X-rays that drive the heating, but it may well be that it is the photosphere of the primary star itself that is important. The spot position $\sim 90°$ ahead of the secondary means that the spot may not be able to see the secondary star at all. This leads to a simple but important modification as we now show.

4.2.2 Heating driven by the primary star's photosphere

If the primary star's photosphere drives the heating then this sets a relation between T_1 and T_{irr}

$$T_{irr}^4 = T_2^4 + \left(\frac{R_1}{a}\right)^2 T_1^4, \tag{3}$$

where T_2 is the temperature of the unheated photosphere of the secondary star, R_1 is the radius of the primary star, a is the orbital separation and we have assumed that all incident flux is absorbed and for simplicity we do not try to account for the range of incident angles over the heated face, but just consider the sub-stellar point. As we said earlier, if T_2 is significant, it is hard to get much of a reflection effect, so we take it to be negligible and therefore

$$T_1 = \left(\frac{a}{R_1}\right)^{1/2} T_{irr}. \tag{4}$$

The masses adopted above give the smallest ratio of a/R_1 leading to $T_1 = 2.58 T_{irr}$. This equation was used to bootstrap from the lower limit on T_{irr} to a new lower limit of T_1, which was then used to place a new lower limit on T_{irr} using the procedure of the previous section. We obtained updated limits as follows: $T_{irr} > 34,800$ K and $T_1 > 90,000$ K. The heated face temperature rises by a factor of 2.4, and so the lower limit on the bolometric luminosity rises by a factor of 33 to $L > 10 L_\odot = 4.0 \times 10^{34}$ ergs s^{-1}. Again comparing with white dwarfs of similar temperature and mass (Bragaglia et al. 1995), the absolute magnitude of the primary star is bounded by $M_V < 8.0$. Given $V = 21.1$

Israel et al. (2002), and assuming that reddening is negligible, we must have $d > 4.2$ kpc. This would place HM Cnc more than 2.5 kpc out of the plane, and it would possibly be a halo object. We note that a halo-like transverse velocity of 200 km s^{-1} and our distance limit imply a proper motion < 0.01 arcseconds/yr, below the limit of 0.02 arcseconds per years placed by Israel et al. (2002).

Our distance limits do not discriminate between accretion models which work best for large distances, in excess of 4 kpc (Bildsten et al. 2006; D'Antona et al. 2006) and the unipolar inductor model which works well for $d < 1$ kpc (Dall'Osso et al. 2006a,b). However, they do suggest that UV observations may have a value in tightening the lower limits upon temperatures and hence the distance.

4.3 Direct impact or polar?

We have lumped the accreting double-degenerate models, direct impact and polar together as "accretion models", as we think they provide equally good explanations for our data. For V407 Vul the double-degenerate polar model suggested by Cropper et al. (1998) was discarded when no polarisation was found (Ramsay et al. 2002). In the case of HM Cnc, Reinsch et al. (2004) have claimed a detection of circular polarisation but at a low level given the faintness of the target (0.5%) that needs confirmation. However, we think that the polar model may have been written off prematurely as there are some very high-field polars which show very little polarisation (AR UMa, Schmidt et al. 1996; V884 Her, Szkody et al. 1995, Schmidt et al. 2001) and strong soft X-ray components, very much like V407 Vul and HM Cnc. It has been suggested that this is because the shocks are buried in these systems, due to the high accretion rates, rather as Marsh & Steeghs (2002) suggested for the direct impact model. Polars show stronger optical line emission than either V407 Vul or HM Cnc, but this is not a strong argument against the polar model since the systems, if they are double degenerates, would be helium-rich and very compact, and so different from normal CVs.

4.4   Period changes in V407 Vul and the G star

We have shown that the G star does not play a direct role in the variability of V407 Vul but it could be gravitationally bound to the variable, in which case it may cause an apparent period change through variable light travel time effects. How significant could this be? Assuming that the G star has mass M, then the maximum acceleration of the binary along the line of sight is $\sim G_c M/a^2$ where a is the separation of the binary and the G star. The subscript c in the gravitational constant is to avoid confusion with the G star. This leads to a quadratic term in the usual $T_0 + PE + CE^2$ ephemeris equal to

$$C = \frac{G_c M P^2}{2ca^2}, \tag{5}$$

where c is the speed of light and P the orbital period. This leads to an apparent rate of period change given by

$$\dot{P} = \frac{G_c M P}{ca^2}. \tag{6}$$

Taking a to be comparable to the projected separation at 1 kpc of 27 AU, and $M = 1 \, M_\odot$ gives $|\dot{P}|_{\max} \sim 1.6 \times 10^{-11}$ s/s. This is about 5 times larger than the observed value (Strohmayer 2005) and thus we conclude that the G star has the potential to have a significant effect upon the rate of period change measured in this system. This adds an extra uncertainty that may allow both the unipolar inductor (Marsh & Nelemans 2005; Dall'Osso et al. 2006a,b) and accreting models (D'Antona et al. 2006) to match this system more easily than has been the case to date. Continued observations in order to place limits upon or detect a relative proper motion between the variable and the G star would be of interest for testing the triple star model. We estimate the orbital velocity of the G star to be $\sim 3 \mathrm{kms}^{-1}$, which is perhaps detectable given a long enough period of time.

5   CONCLUSION

We have presented optical photometry of V407 Vul and HM Cnc in i', r', g' and u' bands taken with the high-speed CCD camera ULTRACAM. For V407 Vul we have a hint of detection of a third component in the system at $0.027''$ from the variable. We believe this to be the G star that is seen in the spectrum of V407 Vul, which therefore cannot be the secondary star of the variable. We cannot distinguish whether it is a line-of-sight coincidence or a triple system.

For HM Cnc we find a new phasing of the X-ray and optical data which renders it indistinguishable from V407 Vul with the optical pulses 0.2 cycles ahead of the X-ray pulses. The offsets are naturally produced by double-degenerate accreting models of the systems, both polar and direct impact, but seem hard to reconcile with the unipolar inductor and intermediate polar models. The optical light curves of HM Cnc are non-sinusoidal and a Fourier decomposition shows that there is likely a contribution to the optical light from the same site as produces the X-rays.

On the assumption that the optical pulses of HM Cnc are the result of irradiation of the secondary star within a double degenerate binary, and using the relative constancy of the fractional pulsation amplitude with wavelength, we place a lower limit on the distance to the system of > 1.1 kpc.

If it is the photosphere of the accretor rather than the X-ray site that is responsible for the heating, then this limit rises to $d > 4.2$ kpc. Space ultraviolet observations are the best hope for strengthening these constraints.

Finally we remark that both the polar and direct impact models provide equally good explanations of our observations and that there are high magnetic field polars that show similar properties to V407 Vul and HM Cnc i.e. very soft X-ray spectra and low polarisation.

REFERENCES

Barros S. C. C., Marsh T. R., Groot P., Nelemans G., Ramsay G., Roelofs G., Steeghs D., Wilms J., 2005, MNRAS, 357, 1306

Bildsten L., Townsley D. M., Deloye C. J., Nelemans G., 2006, ApJ, 640, 466

Bragaglia A., Renzini A., Bergeron P., 1995, ApJ, 443, 735

Burwitz V., Reinsch K., 2001, AIP Conf. Proc. 599: X-ray Astronomy: Stellar Endpoints, AGN, and the Diffuse X-ray Background, 599, 522

Cropper M., 1988, MNRAS, 231, 597

Cropper M., Harrop-Allin M. K., Mason K. O., Mittaz J. P. D., Potter S. B., Ramsay G., 1998, MNRAS, 293, L57

Cropper M., Ramsay G., Wu K., Hakala P., 2004, in Vrielmann S., Cropper M., eds, ASP Conf. Ser. 315: IAU Colloq. 190: Magnetic Cataclysmic Variables REVIEW: Ultra-Short Period Double-Degenerate Binaries. pp 324–+

Dall'Osso S., Israel G. L., Stella L., 2006a, A&A, 447, 785

Dall'Osso S., Israel G. L., Stella L., 2006b, ArXiv Astrophysics e-prints

D'Antona F., Ventura P., Burderi L., Teodorescu A., 2006, ArXiv Astrophysics e-prints

Deloye C. J., Taam R. E., 2006, ArXiv Astrophysics e-prints

Dhillon V., Marsh T., 2001, New Astronomy Review, 45, 91

Hakala P., Ramsay G., Byckling K., 2004, MNRAS, 353, 453

Hakala P., Ramsay G., Wu K., Hjalmarsdotter L., Järvinen S., Järvinen A., Cropper M., 2003, MNRAS, 343, L10

Horne J. H., Baliunas S. L., 1986, ApJ, 302, 757

Israel G. L., Covino S., Dall'Osso S., Fugazza D., Mouche C. W., Stella L., Campana S., Mangano V., Marconi G., Bagnulo S., Munari U., 2004, Memorie della Societa Astronomica Italiana Supplement, 5, 148

Israel G. L., Covino S., Stella L., Mauche C. W., Campana S., Marconi G., Hummel W., Mereghetti S., Munari U., Negueruela I., 2003, ApJ, 598, 492

Israel G. L., Hummel W., Covino S., Campana S., Appenzeller I., Gässler W., Mantel K.-H., et al., 2002, A&A, 386, L13

Israel G. L., Panzera M. R., Campana S., Lazzati D., Covino S., Tagliaferri G., Stella L., 1999, A&A, 349, L1

Lomb N. R., 1976, ASS, 39, 447

Marsh T. R., Nelemans G., 2005, MNRAS, 363, 581

Marsh T. R., Nelemans G., Steeghs D., 2004, MNRAS, 350, 113

Marsh T. R., Steeghs D., 2002, MNRAS, 331, L7

Motch C., Haberl F., Guillout P., Pakull M., Reinsch K., Krautter J., 1996, A&A, 307, 459

Naylor T., 1998, MNRAS, 296, 339

Nelemans G., Portegies Zwart S. F., Verbunt F., Yungelson L. R., 2001, A&A, 368, 939

North R. C., Marsh T. R., Kolb U., Dhillon V. S., Moran C. K. J., 2002, MNRAS, 337, 1215

Norton A. J., Haswell C. A., Wynn G. A., 2004, A&A, 419, 1025

Ramsay G., Cropper M., Hakala P., 2006, MNRAS, 367, L62

Ramsay G., Cropper M., Wu K., Mason K. O., Hakala P., 2000, MNRAS, 311, 75

Ramsay G., Hakala P., Cropper M., 2002, MNRAS, 332, L7

Ramsay G., Wu K., Cropper M., Schmidt G., Sekiguchi K., Iwamuro F., Maihara T., 2002, MNRAS, 333, 575

Reinsch K., Burwitz V., Schwarz R., 2004, in Tovmassian G., Sion E., eds, Revista Mexicana de Astronomia y Astrofisica Conference Series On the Nature of the Binary Components of RX J0806.3+1527. pp 122–123

Scargle J. D., 1982, ApJ, 263, 835

Schmidt G. D., Ferrario L., Wickramasinghe D. T., Smith P. S., 2001, ApJ, 553, 823

Schmidt G. D., Szkody P., Smith P. S., Silber A., Tovmassian G., Hoard D. W., Gänsicke B. T., de Martino D., 1996, ApJ, 473, 483

Schwarzenberg-Czerny A., 1998, MNRAS, 301, 831

Steeghs D., Marsh T. R., Barros S. C. C., Nelemans G., Groot P. J., Roelofs G. H. A., Ramsay G., Cropper M., 2006, ApJ, 649, 382

Strohmayer T. E., 2002, ApJ, 581, 577

Strohmayer T. E., 2003, ApJ, 593, L39

Strohmayer T. E., 2004, ApJ, 610, 416

Strohmayer T. E., 2005, ApJ, 627, 920

Szkody P., Silber A., Hoard D. W., Fierce E., Singh K. P., Barrett P., Schlegel E., Piirola V., 1995, ApJ, 455, L43+

Wu K., Cropper M., Ramsay G., Sekiguchi K., 2002, MNRAS, 331, 221

t_0 (TDB)	49257.533373137
ϕ_0	0.003(30)
ν (Hz)	0.00175624626(39)
$\dot{\nu}$ (Hz s^{-1})	$9.9(1.9) \times 10^{-18}$
$r(\phi_0, \nu)$	-0.92074289
$r(\phi_0, \dot{\nu})$	0.86174740
$r(\nu, \dot{\nu})$	-0.98817908

Table A1. Ephemeris of V407 Vul derived from the data of Ramsay et al. (2006).The uncertainties of the parameters are given within parentheses. We also give the correlation coefficients for the fitted parameters.

APPENDIX A: EPHEMERIDES

A0.1 *V407 Vul's ephemeris*

As we mentioned in Section 3.1, in order to calculate the uncertainty in the published ephemerides we need the covariance terms of the fitted coefficients that are not given in any published work. Therefore we had to digitise and fit the X-ray data in order to obtain a timing solution whose uncertainties we could compare with our data. To digitise the data we applied the Linux utilities *pstoedit* and *xfig* to the PostScript figures from the published papers to obtain the coordinates of the points and their error bars. Such a process can at best match the original data, and can potentially degrade it, but in this case the precision of the PostScript data is good enough that it has no measurable effect; we were able to confirm our numbers directly in one case after Dr Ramsay kindly sent us his data. For V407 Vul's ephemeris we digitised the bottom panel of Figure 6 from Strohmayer (2004) and Figure 1 from the recently published ephemeris of Ramsay et al. (2006) that extends the ephemeris to April 2004. These figures show the residuals in phase relative to a given timing solution. In each case we applied the given timing solution to the observation times and added the phase residuals to obtain the phases as a function of time. We then fitted a timing solution similar to the one used by Strohmayer (2004), i.e. $\phi(t) = \phi_0 + \nu(t - t_0) + \dot{\nu}(t - t_0)^2/2$. We included an extra term (ϕ_0) because we fixed t_0 to be the same as Strohmayer (2004), so this value is no longer arbitrary. We obtain the same fitted parameters as Strohmayer (2004) but slightly different parameters to those of Ramsay et al. (2006). For reasons we shall explain, it is our fit to the data of Ramsay et al. (2006) that is given in Table A1. This corresponds to $\dot{P} = -3.21(61) \times 10^{-12}$ s s^{-1} which can be compared with the value $\dot{P} = -3.31(09) \times 10^{-12}$ s s^{-1} from Ramsay et al. (2006). Our uncertainty is six times larger than that of Ramsay et al. (2006) and the values are slightly different because we allowed more freedom in the fit. We think our fit is the correct one because there is no reason that the fit has to have zero value and gradient at $t = 0$, as was effectively assumed by Ramsay et al. (2006), who fitted only a parabolic term.

Comparing the two ephemerides we found that the value of the frequency derivative was not consistent. Moreover if we calculate the phase of the maximum of our observation with the ephemeris from Strohmayer we obtain 0.8170 ± 0.0016 for the May 2003 and 0.7328 ± 0.0013 for August 2005 (different from 0.97 of Table 6 from Ramsay et al.

2006). This suggests that the two ephemerides have different zero points contrary to what was stated in the respective papers. Next we compared the phases predicted by the two ephemerides expecting to see a constant offset between the two. Instead we found a drift between one ephemeris and the other. The phase difference started at approximately zero for the first observation with ROSAT (so indeed the two ephemerides had exactly the same zero point) but were 0.15 cycles apart for the last Chandra observation. Therefore we re-analysed the ROSAT data from the 30th April 1996 and phase-folded it on Strohmayer's (2004) ephemeris, but obtained the same phasing as Ramsay et al. (2006). We can only obtain the same phasing as Strohmayer (2004) if we do not apply the UTC to TT correction. In the ROSAT documentation it says that the times are in UTC[1]. The error in the ROSAT times causes Strohmayer (2004) to underestimate the rate of spin-up in V407 Vul, and this is why his frequency derivative is lower than that of Ramsay et al. (2006).

To be sure of the correct phasing between the X-ray and optical light curves of V407 Vul we used Table A1's ephemeris and applied it to Chandra data taken on 19th of February 2003 and 24th November 2003, which were taken before and after our May 2003 observation. We obtained the same relative phasing of the optical and X-rays at each epoch. When we use the ephemeris of Ramsay et al. (2006), the two Chandra X-ray light curves are almost perfectly aligned (Figure 5), but if we use Strohmayer's ephemeris, there is a distinct shift between them. We take this as further evidence of a problem with Strohmayer's ephemeris.

To conclude, we used the ephemeris that resulted from refitting the data Ramsay et al. (2006) to give the ephemeris listed in Table A1. In the top panel of Figure A1 we show the residuals of our fitted phases for V407 Vul after removal of a constant frequency model with $\nu_0 = 0.0017562482721063$ Hz. We also show the fitted parabola minus the linear fit.

For V407 Vul we performed an F-ratio test for the parabola versus the linear fit. The χ^2 value of the parabola is 23.4 and of the linear fit is 115, we have 10 points so we obtain an F-ratio=4.33 which is significant at the 95% confidence level but not at 99%.

A0.2 HM Cnc's ephemeris

As was explained above in the case of V407 Vul, in order calculate the uncertainties in phase due to the ephemeris we need to know the covariance terms of the ephemeris. Therefore we applied the same method as before and digitised and fitted the data of Figure 7 of Strohmayer (2005). We obtained the same fit coefficients as Strohmayer (2005) so our digitisation does not cause loss of information; in this case no ROSAT data were involved. We also obtain the covariance terms. Our fitted parameters are given in Table A2. We show the phase residuals after subtracting a constant frequency model ($\nu_0 = 0.0031101279743869$ Hz) in the bottom panel of Figure A1. We applied an F-ratio test to the HM Cnc data. This time there were 69 points and we obtained a χ^2 of 54.9 for the parabolic fit and 10380 for the
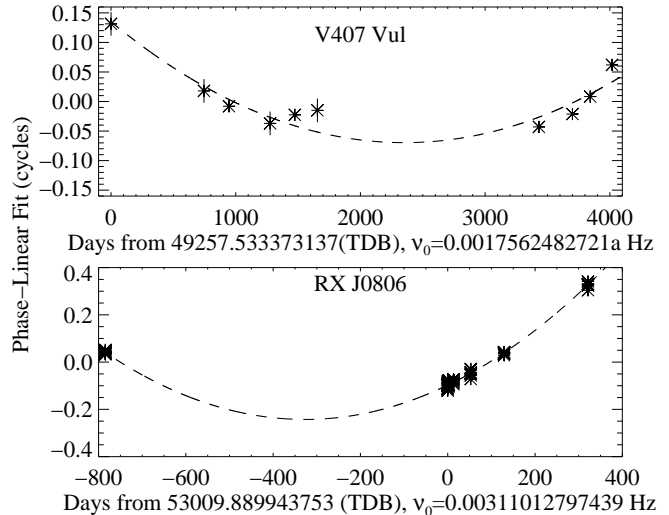
Figure A1. Phase residuals of V407 Vul (top panel) and HM Cnc (bottom panel) after subtraction of constant frequency models. The dashed line shows our parabola ephemeris subtracted the linear fit.

t_0 (TDB)	53009.889943753
ϕ_0	0.0003(14)
ν (Hz)	0.00311013824(10)
$\dot{\nu}$ (Hz s^{-1})	$3.63(0.04) \times 10^{-16}$
$r(\phi_0, \nu)$	-0.48041115
$r(\phi_0, \dot{\nu})$	-0.61096603
$r(\nu, \dot{\nu})$	0.94898169

Table A2. Ephemeris of HM Cnc derived from Figure 7 of Strohmayer (2005) . The uncertainties of the parameter's are given within brackets. We also give the correlation coefficients for the fitted parameters.

linear fit. This gives an F-ratio of 186, significant at the 99.99% confidence level.

A0.3 Uncertainties on phases from the ephemerides

To calculate the uncertainties in the absolute phases due the uncertainties in the ephemeris we used the relation:

$$\sigma_\phi^2 = \sigma_{\phi_0}^2 + (t - t_0)^2 \sigma_\nu^2 + (t - t_0)^4 \sigma_{\dot\nu}^2/4 + \\ 2(t - t_0)C_{\phi_0\nu} + (t - t_0)^3 C_{\nu\dot\nu} + (t - t_0)^2 C_{\dot\nu\phi_0} \quad \text{(A1)}$$

where C_{XY} is the covariance of X and Y and can be written $C_{XY} = \sigma_X \sigma_Y r(X, Y)$. We give the correlation coefficients $r(X, Y)$ in Table A1 and Table A2.

For the phase difference between two epochs $\Delta\phi = \phi(t_2) - \phi(t_1)$ one cannot simply combine in quadrature the uncertainties on the absolute phases at each epoch because the same coefficients are used in each case. (This is most easily seen by considering the case of two identical epochs for which the uncertainty in the phase difference must be zero.) Instead one must use the following relation:

$$\sigma_{\Delta\phi}^2 = (t_2 - t_1)^2 \sigma_\nu^2 + [(t_2 - t_0)^2 - (t_1 - t_0)^2]^2 \sigma_{\dot\nu}^2/4 + \\ (t_2 - t_1)[(t_2 - t_0)^2 - (t_1 - t_0)^2]C_{\nu\dot\nu}. \quad \text{(A2)}$$

We used this to calculate the uncertainties on the phase differences in sections 3.2 and 3.4.